JVSTB Journal of Vacuum Science & Technology B

FeGe liquid metal ion source for maskless isolation implants in InP

C. H. Chu, D. L. Barr, L. R. Harriott, and H. H. Wade

Citation: Journal of Vacuum Science & Technology B **10**, 1273 (1992); doi: 10.1116/1.585899
View online: http://dx.doi.org/10.1116/1.585899
View Table of Contents: http://scitation.aip.org/content/avs/journal/jvstb/10/4?ver=pdfcov
Published by the AVS: Science & Technology of Materials, Interfaces, and Processing

Articles you may be interested in
Mechanisms for the activation of ion-implanted Fe in InP
J. Appl. Phys. **100**, 023539 (2006); 10.1063/1.2220000

Structural and magnetic properties of Fe–Ge layer produced by Fe ion-implantation into germanium
J. Appl. Phys. **91**, 1410 (2002); 10.1063/1.1427135

Redistribution of Fe and Ti implanted into InP
J. Appl. Phys. **70**, 2604 (1991); 10.1063/1.349370

Effects of background Fe concentrations in the annealing of ionimplanted Si into InP substrates for InP metal insulatorsemiconductor fieldeffect transistor applications
J. Appl. Phys. **66**, 1855 (1989); 10.1063/1.344359

Annealing behavior of ionimplanted Fe in InP
J. Appl. Phys. **58**, 1698 (1985); 10.1063/1.336040

Re-register for Table of Content Alerts

Create a profile.
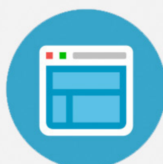
Sign up today!

Redistribution subject to AVS license or copyright; see http://scitation.aip.org/termsconditions. Download to IP: 140.113.38.11 On: Thu, 01 May 2014 14:08:45

FeGe liquid metal ion source for maskless isolation implants in InP

C. H. Chu,[a] D. L. Barr, L. R. Harriott, and H. H. Wade
AT&T Bell Laboratories, Murray Hill, New Jersey 07974

(Received 23 September 1991; accepted 28 April 1992)

A Fe–Ge alloy was used to fabricate a liquid metal ion source (LMIS) for our focused ion beam system. The iron ion and germanium ions can be utilized to create semi-insulating regions for device isolation and n-type doping in InP. The properties of the Fe–Ge LMIS were characterized by measuring the ion current-extraction voltage characteristics, the mass spectrum of the ion species in the ion beam, and the stability of the source current. The changes of resistivity in InP before and after Fe^{++} implant and after thermal annealing were measured in mesa-etched four-terminal test structures. The resistivity of as-implanted samples increases about four orders of magnitude compared with original resistivity. After rapid thermal annealing at 400 °C for 10 s, the resistivity is about two times larger than that of as-implanted sample.

I. INTRODUCTION

Liquid metal ion sources (LMIS) have high brightness, small virtual source size, and a moderate energy spread making them suitable for probe forming systems with beam diameters of 0.1 μm or less. Applications of focused ion beam (FIB) systems cover a wide range of processing techniques in industry and research.[1] One of these applications is maskless isolation implants in compound semiconductors.[2] It is important to provide device isolation by forming semi-insulating regions in compound semiconductors. High resistivity is obtained either through defect-induced compensation or through carrier trapping by deep level impurities.[3] However, defect-induced compensation generally cannot withstand high temperature processing.[4–9] The point defects induced by the ion implantation are subjected to annealing. Carrier trapping and compensation by deep level impurities which are incorporated into the substrate by ion implantation are able to withstand high temperature processing. Bulk semi-insulating InP is generally obtained by doping with Fe. The role of iron as a compensating deep acceptor level with an energy level located about 0.65 eV below the conduction band edge,[10] near the center of the band gap, in bulk n-InP has been extensively studied,[11–14] and is responsible for the semi-insulating properties of Fe:InP. In this study, an iron-germanium alloy was synthesized as a LMIS for maskless focused ion beam isolation implantation in InP.

II. EXPERIMENTAL PROCEDURES

Due to its high melting temperature, Fe is difficult to use directly as a LMIS in a FIB system. An alloy system has to be used to lower the melting point and to satisfy the requirements of a successful LMIS.[15] The Fe–Ge system was chosen because of the wide composition region in the eutectic transformation. Figure 1 shows the phase diagram of this Fe–Ge system.[16] The atomic concentrations of germanium in this region are about 69%–76% and the melting temperatures are 840–838 °C. The Fe–Ge alloy was synthesized by melting Fe powder and a Ge wafer in an arc furnace. The alloy is then put into an Al_2O_3 crucible and homogenized at 950 °C in a vacuum furnace at a pressure of 10^{-7} Torr. A small piece of Fe–Ge alloy was then placed on the tungsten LMIS structure and melted by applying filament current. After that, this emitter was operated to obtain the emission current-extraction voltage characteristics, mass spectrum of the ion beam, and the source current stability.

The isolation implant of focused Fe^{++} ions was performed in our JEOL JIBL-104 UHV focused ion beam system with 100 kV accelerating voltage. The mass spectrum obtained from the EXB mass separator in our machine is shown in Fig. 2. Separation of iron isotopes was not achieved. During the implantation, doubly charged iron ions were used. The implant doses ranged from 7.5×10^{13} to $4.5\times10^{14}/cm^2$. Semi-insulating InP substrates with molecular beam epitaxial grown 100-nm-thick n-type InP were mesa etched to delineate the four-terminal test structure. Ohmic contacts were formed by depositing and alloying Au–Sn–Au metal layers. Resistances were measured from the same test structures before and after isolation implant and also after 400 °C, 10 s rapid thermal annealing (RTA)

III. RESULTS AND DISCUSSION

A. Characterization of Fe–Ge LMIS

The total ion current versus extraction voltage curve is shown in Fig. 3. Ion emission started at 3 keV and the ion current increased with the extractor voltage. Hysteresis was observed in the I–V characteristic by sweeping the extractor voltage back and forth. This is a typical I–V characteristic observed from emission of LMIS. The hysteresis is due to the flow impedance of the molten alloy, which cannot follow the change of electric field near the tip. The flow impedance depends on several parameters such as the presence or absence of grooves at the lateral surface of the needle, the length of the needle, and its apex radius.[17,18]

Ion species of the Fe–Ge LMIS were analyzed in a mass analyzer. Figure 4 shows the mass spectrum of ions emitted from the Fe–Ge LMIS, which was measured by using a sector magnet and a Faraday cup. Singly and doubly charged ^{56}Fe and ^{74}Ge were the dominant ion species emitted from the Fe–Ge LMIS. Molecular ions, complex ions, and isotopes of Fe and Ge were also observed. The ratio of

 0734-211X/92/041273-04$01.00 ©1992 American Vacuum Society

Redistribution subject to AVS license or copyright; see http://scitation.aip.org/termsconditions. Download to IP: 140.113.38.11 On: Thu, 01 May 2014 14:08:45

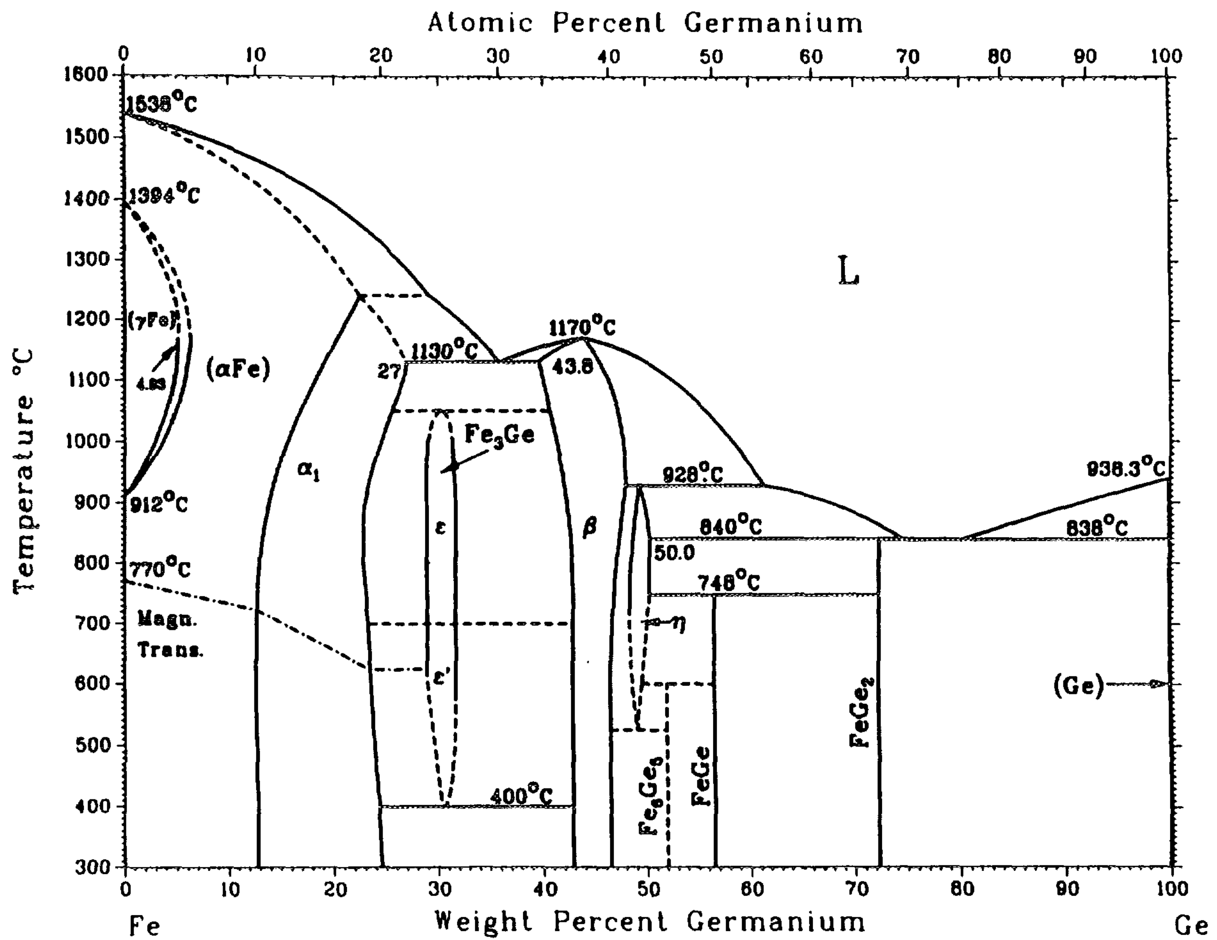

FIG. 1. The binary phase diagram of Fe–Ge system.

Ge/Fe in the bulk LMIS measured by x-ray fluorescence was 2.2, which closely matched the ratio of 2.13 observed in the ion beam. The result indicates that there is a little germanium deficiency in the ion beam which gradually increases the composition of Ge in the source. Therefore, we prepared the Fe–Ge alloy with bulk composition of $FeGe_{2.2}$ to keep the melting temperature constant during source operation.

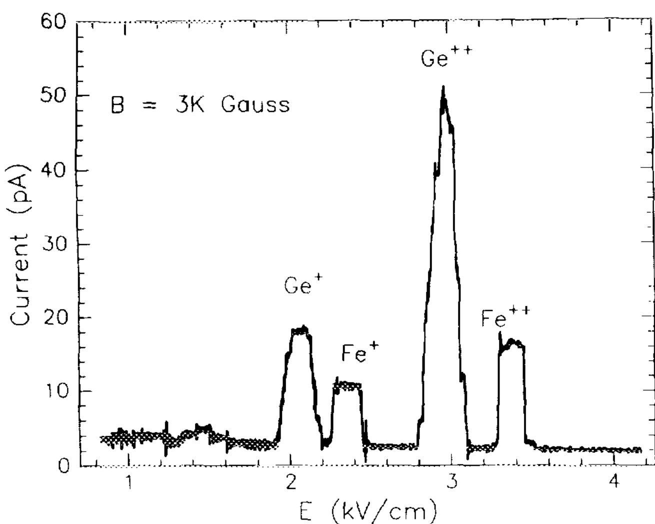

FIG. 2. The mass spectrum of Fe–Ge LMIS obtained from the EXB mass separator in our JOEL JIBL-104 UHV FIB system.

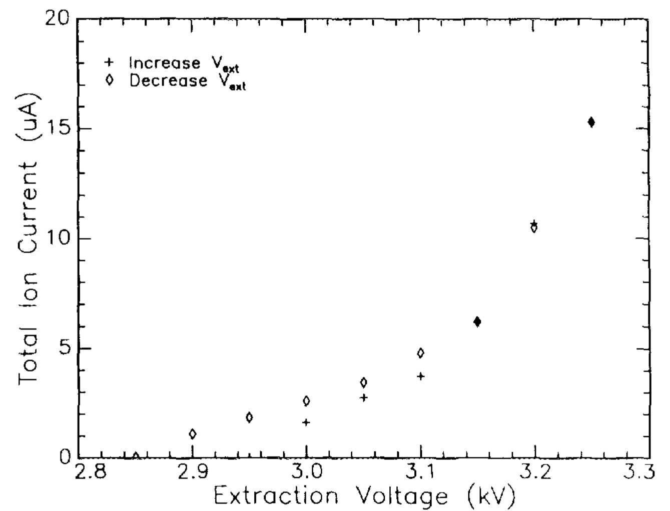

FIG. 3. *I–V* characteristics of Fe–Ge liquid metal ion source using tungsten as the base.

Redistribution subject to AVS license or copyright; see http://scitation.aip.org/termsconditions. Download to IP: 140.113.38.11 On: Thu, 01 May 2014 14:08:45

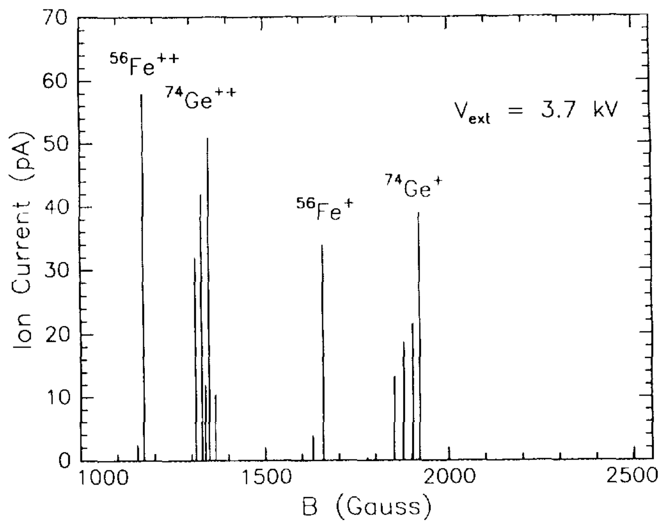

FIG. 4. Mass spectrum of ions emitted from the Fe–Ge liquid metal ion source measured by sector magnet mass analyzer.

The stability of the source current was measured after 1 h operation. Figure 5 shows the stability of the $^{56}Fe^{++}$ ion current, which was obtained by the sector magnet, over a 1 h period under constant extraction voltage. The fluctuation of the $^{56}Fe^{++}$ ion current was about 5%.

The reaction of the Fe–Ge alloy with the W filament substrate was studied by energy dispersive spectroscopy (EDS). The morphologies of the W filament before putting the Fe–Ge alloy on and at the end of source life were investigated in a scanning electron microscope as shown in Fig. 6. Elongated tungsten grains along the direction of the W wire were changed into granular grains due to the recrystallization which was induced by the high temperature during the source operation. The composition of the areas surrounding tungsten grains probed by the electron beam is determined to be germanium. During the operation of the LMIS, germanium penetrated into the W substrate via the W grain boundaries. The penetration of the germanium finally weakens the tungsten substrate and reduces the lifetime of the source.

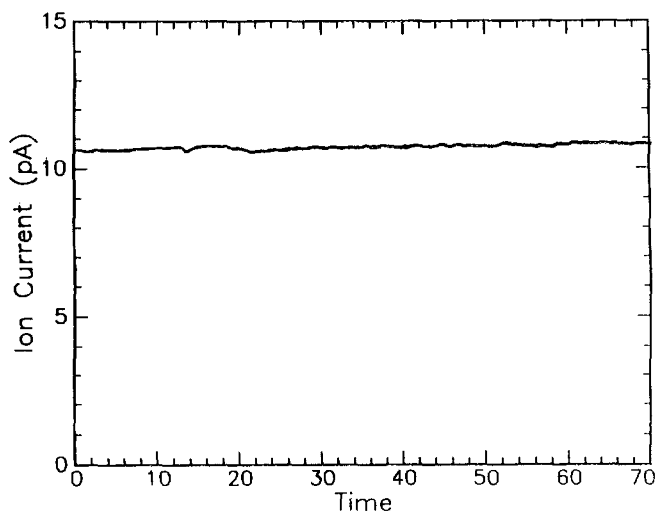

FIG. 5. Ion beam stability of Fe–Ge liquid metal ion source after 1 h of operation.

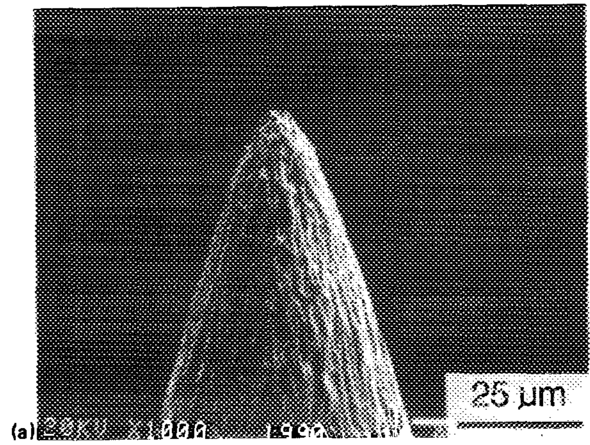

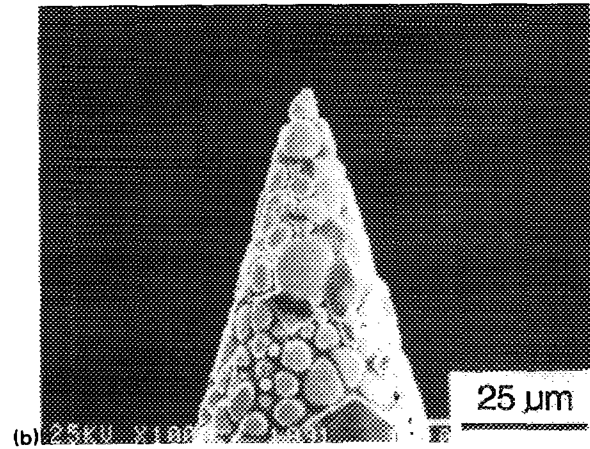

FIG. 6. Secondary electron images of tungsten tips (a) prior to coating with $FeGe^{2.2}$ and (b) after the source material has been exhausted.

B. Maskless isolation implant of Fe^{++} in InP

The resistance of *n*-type InP was measured by using the four-terminal test structure as shown in Fig. 7. Sizes of implanted areas are 30×5 and 30×10 μm^2. The projected range of 200 keV iron ions is about 123 nm, which is deep enough for the ions to penetrate into the semi-insulating substrate and isolate the current conducting layer. Resistances measured before and after Fe^{++} isolation implant and after 400 °C RTA for 10 s, are shown in Table I. Before the Fe^{++} implant, resistances measured from different areas were around 2.5 kΩ. Converting the resistance into resistivity, it shows that the resistivity of the *n*-type InP layer is about 0.025 Ω cm. After Fe^{++} implantation, resistances increased to about 10 MΩ. Resistances measured in the as-implanted samples decrease as the implant dose increases. Reports show that there is an optimum dose to obtain the maximum resistance.[6,8,9] Two mechanisms have been suggested to explain the decrease of resistance in the high dose implanted samples: the banding of defect levels[8] and the onset of hopping conduction.[19] After

Redistribution subject to AVS license or copyright; see http://scitation.aip.org/termsconditions. Download to IP: 140.113.38.11 On: Thu, 01 May 2014 14:08:45

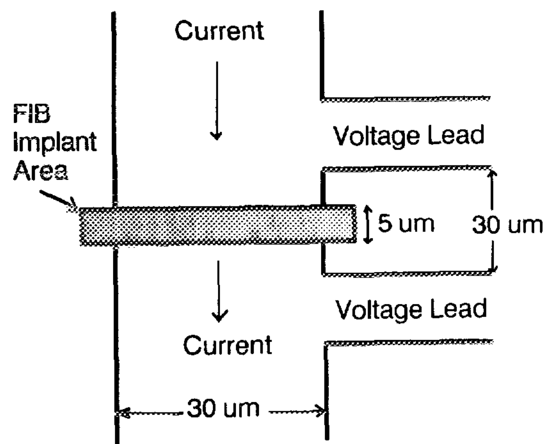

FIG. 7. Schematic diagram of the four-terminal test structure utilized to measure the changes of resistance of n-InP after implant and annealing.

annealing at 400 °C for 10 s, most of the samples showed an increase of resistance. The samples with higher implant dose have higher resistance.

Due to the damage induced levels in InP appearing in the upper-half of the band gap, it is very difficult to produce high resistivity regions in n-type InP.[20] The resistivities which were induced by defect levels in ion implanted InP were reported from 10^2 to 10^4 Ω cm.[4–6,8,9] Resistances measured from our samples before annealing fall into this range and indicate that the increase of resistance could be due to the damage induced by the Fe^{++} implantation. For He^+, H^+, Be^+, and B^+ implanted samples, the resistivities drop to the original value after 400 °C annealing (in order to prevent melting of the ohmic contact alloy, the annealing temperature is limited to below 400 °C in our studies). Solid phase epitaxial regrowth (SPER) of amorphous InP was observed to take place below 250 °C but left a high level of residual damage. Annealing at 450 °C removes most of the lattice damage.[21–23] In our studies with a 400 °C annealing temperature, the temperature is high enough to finish SPER and partially recover the damage. The high resistances measured after annealing indicate that partial activation of Fe is obtained. The increase of resistivity in Fe doped n-type InP has been reported to be as high as 10^7 Ω cm.[7] The resistivities obtained in our annealed samples are around 600 Ω cm. This may be caused by the redistribution of Fe, partial activation of Fe, and partial recovery of lattice damage. Iron pileup at the original amorphous/crystalline has been observed from the secondary ion mass spectrometry in annealed room temperature Fe^+ implanted InP.[24] The redistribution of Fe in InP depends on the degree of damage, the Fe concentration, the background doping concentration, and the annealing condition. In order for us to achieve the maximum resistivity, continuing efforts have to be made to optimize the Fe^{++} FIB implantation and annealing conditions.

TABLE I. Resistances measured from four-terminal test structure of n-InP/SI–InP before and after Fe^{++} implantation and after rapid thermal annealing.

Areas (μm^2)	n-InP (kΩ)	As implanted 200 keV,Fe^{++} (MΩ)	RTA 400 °C, 10 s (MΩ)	Dose (cm^{-2})
30×5	2,45	8.9	18.5	1.5×10^{14}
30×10	2.58	8.5	20.0	3.0×10^{14}
30×10	2.40	10.5	13.7	1.5×10^{14}
30×10	2.47	13.0	10.6	7.5×10^{13}

IV. SUMMARY AND CONCLUSION

In summary, a $FeGe_{2.2}$ LMIS has been successfully fabricated for maskless isolation implantation in InP material. The dominant ion species obtained from the ion beam are singly and doubly charged ^{56}Fe and ^{74}Ge. The ion current fluctuation measured from the stability test of $^{56}Fe^{++}$ was about 5% under constant extraction voltage. The resistivities measured after maskless FIB iron implantation and 400 °C annealing increase about four orders of magnitude as compared with the original resistivity.

ACKNOWLEDGMENTS

The authors would like to thank H. Chou and P. L. Trevor for their help in EDS and x-ray fluorescence analyses.

[a)]Present address: National Nano Device Laboratory at National Chiao Tung University, Hsinchu, Taiwan, Republic of China.

[1]L. R. Harriott, in *VLSI Electronics: Microstructure Science* (Academic, New York, 1989), Vol. 21.
[2]A. D. Wieck and K. Ploog, Appl. Phys. Lett. **56**, 928 (1990).
[3]B. G. Streetman and A. Dodabalapur, Mater. Res. Soc. Symp. Proc. **126**, 159 (1988).
[4]H. Asahi, H. Sumida, S. J. Yu, S. Emura, S. I. Conda, and M. Komuro, Jpn. J. Appl. Phys. **28**, L2119 (1989).
[5]M. W. Focht, A. T. Macrander, B. Schwartz, and L. C. Feldman, J. Appl. Phys. **55**, 3859 (1984).
[6]P. E. Thompson, S. C. Binari, H. B. Dietrich, and R. L. Henry, Solid State Electron. **27**, 817 (1984).
[7]J. P. Donnelly and C. E. Hurwitz, Solid State Electron. **21**, 475 (1978).
[8]J. P. Donnelly and C. E. Hurwitz, Solid State Electron. **20**, 727 (1977).
[9]P. E. Thompson, S. C. Binari, and H. B. Dietrich, Solid State Electron. **26**, 805 (1983).
[10]G. N. Iseler, Inst. Phys. Conf. Ser. No. **45**, 144 (1979).
[11]J. W. Allen, J. Phys. C **2**, 1077 (1969).
[12]G. L. Miller, D. V. Lang, and L. C. Kimmerling, Annu. Rev. Mater. Sci. **7**, 388 (1977).
[13]K. P. Pande and G. G. Roberts, J. Phys. C **9**, 2899 (1976).
[14]J. Cheng, S. R. Forrest, B. Tell, D. Wilt, B. Schwartz, and P. Wright, J. Appl. Phys. **58**, 1780 (1985).
[15]M. J. Bozack, L. W. Swanson, and J. Orloff, Scan. Electron. Microsc. **IV**, 1339 (1985).
[16]O. Kubaschewski, in *Iron-Binary Phase Diagrams* (Springer, New York, 1982).
[17]K. L. Aitken, Proc. Field Emission Day, Noordwijk 23 (1976).
[18]A. Wagner and T. Hall, J. Vac. Sci. Technol. **16**, 1817 (1979).
[19]K. Steeples, I. J. Saunders, and J. G. Smith, IEEE Electron Device Lett. **EDL-1**, 72 (1980).
[20]S. J. Pearton, C. R. Abernathy, W. S. Hobson, and A. E. Von Neida, Mater. Res. Soc. Symp. Proc. **144**, 433 (1989).
[21]P. Zheng, M.-O. Ruault, M. F. Denanot, B. Descouts, and P. Krauz, J. Appl. Phys. **69**, 197 (1991).
[22]D. E. Davies, J. P. Lorenzo, and M. L. Deane, Appl. Phys. Lett. **31**, 256 (1977).
[23]E. F. Kennedy, Appl. Phys. Lett. **38**, 375 (1981).
[24]S. A. Schwarz, B. Schwartz, T. T. Sheng, S. Singh, and B. Tell, J. Appl. Phys. **58**, 1698 (1985).

Redistribution subject to AVS license or copyright; see http://scitation.aip.org/termsconditions. Download to IP: 140.113.38.11 On: Thu, 01 May 2014 14:08:45